Magn Reson Mater Phy (2015) 28:239–249
DOI 10.1007/s10334-014-0460-5

RESEARCH ARTICLE

In vivo proton magnetic resonance spectroscopic imaging of the healthy human brain at 9.4 T: initial experience

Grzegorz L. Chadzynski · Rolf Pohmann · Gunamony Shajan · Rupert Kolb · Sotirios Bisdas · Uwe Klose · Klaus Scheffler

Received: 18 February 2014 / Revised: 22 August 2014 / Accepted: 22 August 2014 / Published online: 24 September 2014

Abstract
Object In this study, the feasibility of in vivo proton magnetic resonance spectroscopic imaging (^{1}H MRSI) of the healthy human brain at a field strength of 9.4 T, using conventional acquisition techniques, is examined and the initial experience is summarized.
Materials and methods MRSI measurements were performed on a 9.4 T MR scanner (Siemens, Erlangen, Germany) equipped with head-only gradient insert (AC84, Siemens) and custom-developed, 8-channel transmit/24-channel receive, and 16-channel transmit/31-channel receive coils. Spectra were acquired from the superior part of the human brain with a modified STEAM sequence. Spectral quantification was done with LCModel software.
Results Reasonable quality and signal-to-noise ratio of the acquired spectra allowed reliable quantification of 12 metabolites (Cramer-Rao lower bounds < 20 %), some of which may be difficult to quantify at field strengths below 7 T due to overlapping resonances or low concentrations.
Conclusion While further developments are necessary to minimize chemical shift displacement and homogeneity of the transmit field, it is demonstrated that in vivo ^{1}H MRSI at a field strength of 9.4 T is possible. However, further studies applying up-to-date techniques to overcome high-field specific problems are needed in order to assess the potential gain in sensitivity that may be offered by MRSI at 9.4 T.

Keywords Spectroscopic imaging · Ultra-high magnetic field · Human brain · Chemical shift displacement · Transmit field inhomogeneities

G. L. Chadzynski (✉) · K. Scheffler
Biomedical Magnetic Resonance, University Hospital Tuebingen, Hoppe-Seyler-Str. 3, 72076 Tübingen, Germany
e-mail: grzegorz.chadzynski@med.uni-tuebingen.de

G. L. Chadzynski · R. Pohmann · G. Shajan · K. Scheffler
High-Field Magnetic Resonance Center, Max Planck Institute for Biological Cybernetics, Spemannstr. 41, 72076 Tübingen, Germany

R. Kolb · S. Bisdas · U. Klose
Diagnostic and Interventional Neuroradiology, University Hospital Tuebingen, Hoppe-Seyler-Str. 3, 72076 Tübingen, Germany

Introduction

In the last years, various reports have confirmed the feasibility of in vivo proton magnetic resonance spectroscopy (^{1}H MRS) and spectroscopic imaging (^{1}H MRSI) at ultra-high magnetic fields (7 T and above), in spite of known difficulties, such as B_0 and B_1 field inhomogeneities, shorter T_2 and longer T_1 relaxation times [1], higher radio-frequency (RF) power deposition and increasing chemical shift displacement errors (CSDE). Overcoming these problems is crucial for MRS/MRSI at ultra-high magnetic fields and often requires both optimized pulse sequences and specific hardware [2].

A comparison between the spectra acquired at 4 T and 7 T revealed that ultra-high magnetic fields offer a significant gain in spectral resolution, which enables the quantification of a larger number of resonances [2, 3, 5], including some that overlap heavily (i.e., glutamine, glutamate, glycine) or whose concentration is difficult to detect at field strengths below 7 T (i.e., taurine, serine, scyllo-inositol or γ-aminobutryic acid) due to insufficient signal-to-noise ratio (SNR) [3, 5, 6]. Specialized techniques have been developed to better differentiate between adjacent resonances [7] or to specifically detect certain metabolites [8–10].

Further increases in SNR and spectral resolution at still higher field strengths might make it possible to detect additional low concentrated metabolites and increase separation between adjacent resonances. This was recently verified by the work of Deelchand et al. [11], where in vivo single voxel spectra at 9.4 T were acquired with a stimulated echo acquisition mode (STEAM) pulse sequence with similar precision of metabolite quantification (Cramer-Rao lower bounds—CRLB) as in previous studies at 7 T, using either STEAM [12] or a spin-echo full-intensity acquired localized (SPECIAL) sequence [6]. However, higher fields cause an increase in the CSDE, resulting in the need to increase the bandwidth of the STEAM localization pulses by 55 % to obtain similar CSDE at 9.4 T as at 7 T [2, 11]. MRSI, on the other hand, avoids in-plane CSDE by using phase encoding gradients, thus reducing its influence to a region close to the edges of the gradient-preselected volume. Recent MRSI studies performed at 7 T demonstrated that even this can be avoided by the use of acquisition schemes without gradient preselection, i.e., by a purely free induction decay (FID)-based MRSI sequence [4, 13, 14]. Moreover, as the main advantage of MRSI over MRS is to provide additional information about the spatial distribution of the measured metabolite resonances, we have examined the possibility of in vivo proton MRSI of the human brain at 9.4 T using STEAM. Here, we summarize the initial experiences with this technique and give indications about possible improvements, especially for minimizing CSDE and transmit field inhomogeneities. To the best of our knowledge, this is the first report describing in vivo MRSI of the human brain at 9.4 T.

Materials and methods

All measurements were performed on a 9.4 T 82 cm horizontal bore whole body MR scanner (Siemens Healthcare, Erlangen, Germany), equipped with a head-only gradient insert (AC84, Siemens) with an inner diameter of 32 cm, maximum gradient strength of 60 mT/m and slew rate of 400 T/m/s. MRSI data were acquired with an 8-channel transmit loop coil combined with a 24-channel array for signal reception (lower resolution measurements), and a 16-channel transmit and 31-channel receive coil combination (higher resolution) [15]. In both cases, the transmit coil operated in circular polarized (CP) mode realized by linearly varying the input phase of the transmit channels as an acceptable compromise between transmit efficiency, specific absorption rate (SAR) and homogeneity of the transmit field over the superior part of the brain.

Five healthy volunteers participated in this study (one female, four males, age 27–44 years, mean: 33 ± 6.5 years), which was approved by the local ethics board. In all in vivo measurements, the SAR averaged over the head mass did not exceed 25 % of the value recommended by the Food and Drug Administration (3.2 W/kg averaged over head mass).

All spectra were acquired with a modified STEAM sequence with the following parameters: repetition time (TR): 2,000 ms, echo time (TE): 20 ms, mixing time (TM): 11 ms, spectral bandwidth: 4,000 Hz, vector size: 2,048 data points, field of view (FOV): 160 × 160 mm^2, volume of interest (VOI): 60 × 60 × 10 mm^3 (at a resolution of 16 × 16 voxels) and 60 × 60 × 15 mm^3 (at a resolution of 32 × 32 voxels), which resulted in a nominal voxel size of 10 × 10 × 10 mm^3 and 5 × 5 × 15 mm^3, respectively. Weighted k-space sampling with up to four averages made it possible to acquire a single data set within 9 min 36 s (low resolution) and 36 min 46 s (high resolution). The k-space sampling scheme caused an increase in the effective in-plane voxel size by a factor of two. The water suppression enhanced through T_1 effects (WET) technique [16] was used for partial suppression of the water peak. The remaining water signal was used as a reference for phase and frequency corrections. Outer volume suppression (OVS) was realized by saturating four slabs around the edges of the VOI. An additional MRSI data set with otherwise identical parameters was acquired without water suppression and used for eddy current correction in LCModel as a preprocessing step, and absolute quantification. B_0 homogenization was performed first by automatic shimming, using the vendor-supplied field map based algorithm, which was repeated until the obtained shim parameters reached stability. The field homogeneity was further improved by manual shimming, where the shim currents were modified to reach the highest possible T_2* and the smallest linewidth of the water signal. The volume selected for shimming (60 × 60 × 10 mm^3 and 60 × 60 × 15 mm^3) was equal to that of the MRSI experiments.

The STEAM-VOI was positioned on anatomical images acquired with a multi-slice gradient-echo sequence (GRE; TR = 302 ms, TE = 9 ms, flip angle: 25°, voxel size: 0.6 × 0.6 × 2 mm^3). GRE slices were positioned in the transverse plane parallel to the line between the anterior and posterior commissures (ac-pc line) above the lateral ventricles. The voltage necessary for the MRSI sequence was determined using flip angle maps acquired with an Actual Flip angle Imaging sequence (AFI; TR1 = 20 ms, TR2 = 100 ms, TE1 and TE2 7 ms, nominal flip angle 60°, voxel size 4.2 × 2.1 × 5 mm^3) [17, 18] and the same slice position and orientation as the anatomical images. The mean flip angle over a slightly (∼1 cm bigger in all directions) larger volume than the MRSI-STEAM VOI was used for calculation of the reference voltage. This allowed optimization of the water suppression and VOI selection

pulses, but resulted in suboptimal settings for the OVS pulses, which were covering a larger area with worse homogeneity of the B_1 field.

The STEAM sequence as implemented on the scanner was slightly modified for the specific requirements of ultra-high field. Namely, Hermite RF pulses were used for excitation and volume selection. This reduced the necessary transmit voltage for the desired 90° flip angle [19]; however, it was at the cost of a less perfect excitation profile (signal loss at the edge of the VOI). In order to reduce CSDE, the used RF pulses were shortened to 1,400 μs (8-channel transmit/24-channel receive coil) and to 1,800 μs (16-channel transmit/31-channel receive coil), which resulted in RF bandwidths of 3,100 and 2,100 Hz, respectively. Finally, the transmitter frequency was set to −2 ppm from the water signal. The resulting CSDE per 3 ppm of the chemical shift range was 39 % (∼8 mm per ppm in-plane and ∼1.3 mm per ppm through-plane) and 57 % (∼10 mm per ppm in-plane and ∼2.9 mm per ppm through-plane) for 8-channel Tx (RF duration of 1,400 μs) and 16-channel Tx (RF duration of 1,800 μs) coils respectively.

For the purpose of visualization, spectra were post-processed offline using custom-developed routines in Matlab (The Mathworks Inc., Natick, MA, USA). Offline spectral post-processing for display consisted of the following steps: zerofilling by a factor of two, apodization with a Hanning function (time constant of 400 ms), fast Fourier transform, manual 0th and 1st order phase correction and baseline correction. The baseline was fitted to those points of the spectrum where no metabolite signal was expected (the following locations were used: ∼4.40, ∼4.28, ∼4.18, ∼3.42, ∼2.94, ∼1.82, ∼1.58, ∼1.11, ∼0.77, ∼0.63 and ∼0.50 ppm), using piecewise cubic Hermite interpolation.

For quantification, data without any spectral post-processing were used. Unprocessed spectra were eddy current corrected and quantified with the LCModel software [20], using a basis set that was simulated with the VeSPA software (http://scion.duhs.duke.edu/vespa/), including the following metabolites: alanine (Ala), aspartate (Asp), Cho, Cr, γ-aminobutryic acid (GABA), glucose (Glc), glutamine (Gln), glutamate (Glu), glycine (Gly), glycerophosphocholine (GPC), glutathione (GSH), myo-inositol (Ins), lactate (Lac), NAA, N-acetylaspartylglutamate (NAAG), phosphocholine (PCh), phosphocreatine (PCr), phosphoryletanolamine (PE), scyllo-inositol (Scyllo), serine (Ser) and taurine (Tau). J-coupling constants and frequencies of metabolite resonances were taken from references [21] and [22], whereas the signals of macromolecules and lipids were simulated with LCModel's predefined parameters (LCModel user's manual version 6.2-4B). Both basis-set simulation and quantification procedures accounted for time parameters (TE, TR) of the MRSI-STEAM sequence, T_1 weighting of the spectra [11], the volume of the MRSI voxel (setting of VOLUME and TRAMP parameters, as described in LCModel user's manual version 6.2-4B), and the water signal for the cerebrospinal fluid content in gray matter [23].

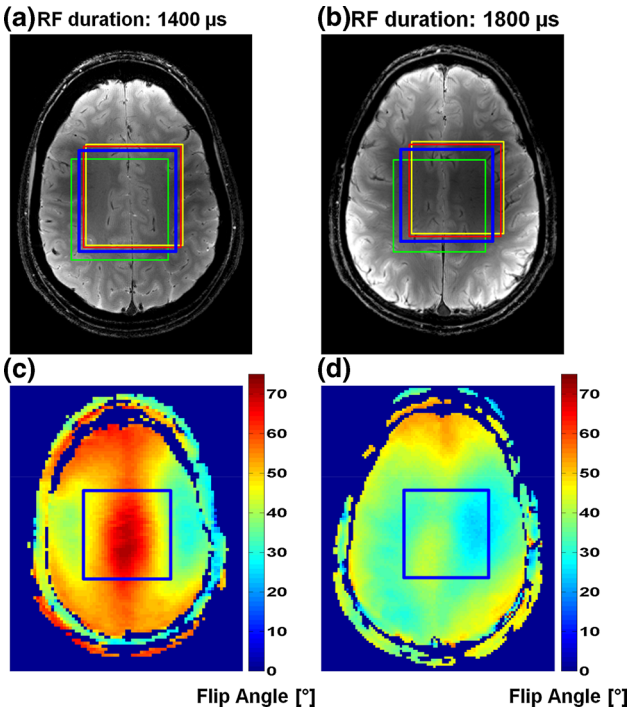

Fig. 1 Gradient-echo scout images (**a**, **b**) and flip angle maps (**c**, **d**) obtained for measurements with an 8-channel transmit/24-channel receive (**a**, **c**) and a 16-channel transmit/31-channel receive (**b**, **d**) coil combination. The position of the VOI for MRSI was marked by a *blue square*. Scout images demonstrate the scale of CSDE at RF pulse duration of 1,400 (**a**) and 1,800 μs (**b**) calculated for tNAA (*green*), tCho (*yellow*), and tCr (*red*). For both volunteers, the flip angle maps were obtained with an AFI sequence at a reference voltage of 300 V and with a targeted nominal flip angle of 60°

Results

Figure 1 shows gradient-echo scout images demonstrating the scale of CSDE calculated for the different RF pulse durations (Fig. 1a—1,400 μs, b—1,800 μs) and the flip angle maps acquired for both coils for a nominal flip angle of 60°. While the targeted flip angle was reached in the center of the slice, it dropped by approximately 40 % towards the edges of the brain, starting from ∼65° to ∼45° and from ∼55° to ∼35° for 8-channel Tx (RF duration of 1,400 μs) and 16-channel Tx (RF duration of 1,800 μs) coils, respectively (Fig. 1c, d). The maximum B_1 fields achieved in the center of the displayed flip angle maps were: 10.5 and 6.0 μT, whereas the minimal B_1

values reached on the right of the brain were: 4.3 and 3.0 μT for 8-channel Tx and 16-channel Tx coils, respectively, similar as in the other volunteers. While the shape of the transmit field distribution was similar with both coils (Fig. 1c, d), the higher transmit efficiency of the 8-channel Tx/24-channel Rx coil can mainly be attributed to differences in geometry between the two coils. In the 16-channel Tx coil, the receive elements were arranged in two rows to provide better coverage and larger excitation volume. This however, distributes the available RF pulse power over a larger volume and shifts the region of maximal B_1 field efficiency in a caudal direction (slightly below the lateral ventricles) [15]. In contrast, the transmit elements of the 8-channel Tx coil were arranged in a single row, which provides worse coverage, but results in a higher transmit field in the region that was examined in this study. For the MRSI experiments, the VOI was therefore placed in the central part of the slice (Fig. 1, marked with blue square), where B_1 was strongest.

Results from a representative volunteer are presented in Fig. 2. The VOI was positioned in transverse orientation, parallel to the ac-pc line, right above the corpus callosum (Fig. 2a). Here, the spectra collected at lower spatial resolution and at RF pulse duration of 1,400 μs (Fig. 2b, c) are displayed. Due to the relatively high bandwidth of the excitation pulses, CSDE is sufficiently reduced to yield a consistent spatial distribution of the resonances of NAA-CH_3 ($\sim$2.02 ppm), total Cho ($\sim$3.2 ppm) Cr-CH_3 ($\sim$3.03 ppm) and macromolecules (between $\sim$1.8 and $\sim$0.8 ppm) within the presented 4 × 4 voxel area (Fig. 2b). Slight CSDE effects may still be visible, especially for NAA in the upper right corner of Fig. 2b, while all spectra within the central 4 × 4 voxels present good quality in terms of SNR and spectral resolution. Figure 2c shows a single spectrum from this particular volunteer. Reasonable SNR and spectral resolution made it possible to distinguish between metabolites that typically overlap at field strengths below 7 T, especially between $\sim$2.1 and $\sim$2.9 ppm, and between $\sim$3.4 and $\sim$4.2 ppm where the signals of Ins, Glu, Gln and NAA are well separated. In this spectrum (Fig. 2c), it is also possible to identify smaller resonances such as Tau, Asp and GABA; however, the latter two metabolites could not be quantified in all subjects. Spectra measured for the other volunteers were similar in terms of quality. The average SNR for spectra from all volunteers (within the central 2 × 2 voxel area), determined from the lower resolution MRSI as the ratio between the maximum of the tCr peak at $\sim$3.03 ppm minus baseline and the root mean square of noise located between 0.2 and 0.4 ppm, was 56.8 ± 13.4, while the average full-width at half maximum (FWHM) calculated again across all the subjects (for the same area of VOI) was 14.6 ± 1.3 Hz. The variations in SNR and FWHM within the area of VOI, calculated again as an average across all volunteers, were $\sim$35 and $\sim$15 %, respectively. Both SNR and FWHM were calculated for non-apodized spectra. Since the amplitude of the metabolite resonances measured at lower spatial resolution showed a uniform distribution over the central 2 × 2 voxel area, those spectra do not show any apparent CSDE within the image plane and were used for further analysis and quantification.

Measurements with higher spatial resolution confirmed the above observations. Figure 3 shows an example of spectra and calculated metabolite maps at higher spatial resolution and with an RF duration of 1,800 μs. Again, despite of the RF duration used, the remaining influence of CSDE can still be seen within the presented 6 × 6 voxel matrix of MRSI spectra (Fig. 3b), as well as in the metabolite maps (Fig. 3c), which shows reduced concentrations of Glu and tCr at the edges of the central 8 × 8 voxel area of VOI (mainly white matter), whereas the regions of higher concentration are located more centrally (mostly gray matter). For Glu, however, the regions of low concentration at the edges of VOI correspond to the regions with high CRLBs (Fig. 4c), suggesting lower fitting quality in this area. For tCr, the CRLB map (Fig. 4c) shows a more uniform distribution (CRLBs <10 %), which indicates a good quality of fit. This, and the fact that CSDE for tCr was relatively low (compared to the other metabolites, see Fig. 1a, b), suggests that this particular metabolite map can to some extent reflect the gray to white matter differences in the concentration of tCr. In contrast, the remaining influence of CSDE on the spatial distribution of NAA and Ins is much stronger and also directly visible.

Figure 4 shows the results of quantification with LCModel. Displayed are the results obtained for single spectra measured at low (Fig. 4a) and high (Fig. 4b) spatial resolution, and CRLB maps obtained for the spectra from the central 8 × 8 area of VOI measured with high resolution. It can be seen that for the first spectrum (acquired at low spatial resolution, Fig. 4a, table on the right) it was possible to quantify 12 of 21 metabolites included in the basis-set with Cramer-Rao lower bounds (CRLB) below 20 %, namely: Cr, GABA, Gln, Glu, Gly, GSH, Ins, NAA, NAAG, PCr, PE and Tau. As for the second spectrum (higher spatial resolution, Fig. 4b, table on the right) it was still possible to assess ten metabolites (CRLB < 20 %) in spite of the lower SNR (75.1 obtained for the spectrum seen in Fig. 4a, versus 30.1 for the spectrum in Fig. 4b). The robustness of quantification is further visualized by the CRLB maps (Fig. 4c) shown for the same volunteer and VOI as the concentration maps in Fig. 3c. For the evaluated metabolites (tNAA, tCr, Ins and Glu), CRLB was not larger than 15 % in most of the voxels, which indicates reasonable fitting quality. The lowest values can be seen

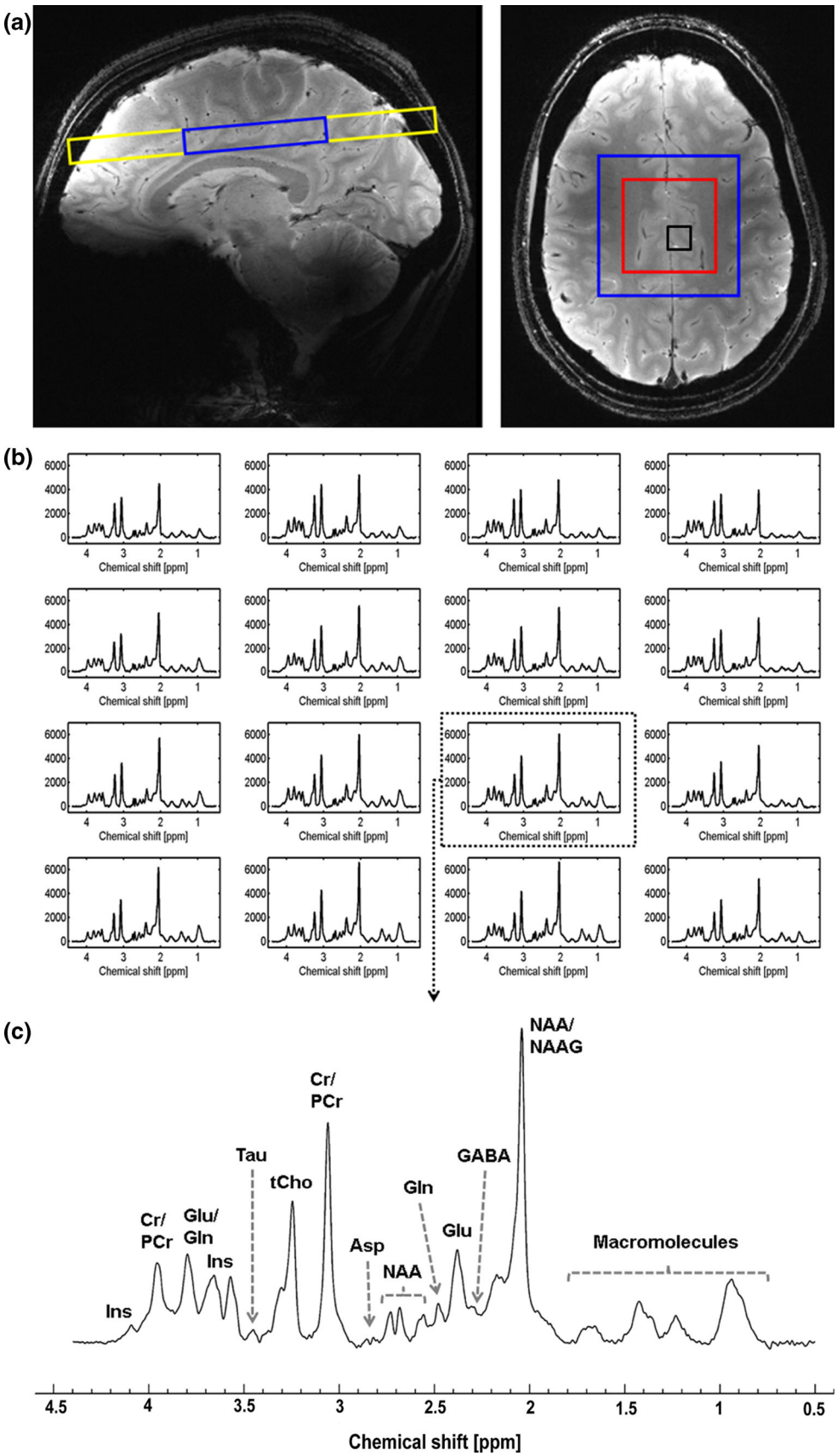

Fig. 2 MRSI results for one representative volunteer measured at low resolution (16 × 16 voxels, nominal voxel size: 10 mm^3 isotropic) with an 8-channel transmit/24-channel receive coil. Gradient-echo scout images (**a**), a 4 × 4 matrix of MRSI spectra (**b**) and a single spectrum (**c**) are shown. The *yellow rectangle* indicates the position of the FOV, whereas the blue square corresponds to the MRSI-VOI. The *red square* seen on the transverse scout shows the 4 × 4 voxel area, the spectra of which are presented below (**b**), while the *black square* marks the localization of the single spectrum shown on the *bottom* (**c**). The presented spectra were zero-filled to 4,096 complex data points, apodized with a Hanning function (time constant 400 ms) and phase, and baseline corrected. For this particular volunteer, the average SNR and FWHM calculated for the tCr peak across the presented 4 × 4 voxel area were 55.0 ± 4.5 and 13.7 ± 0.2 Hz, respectively

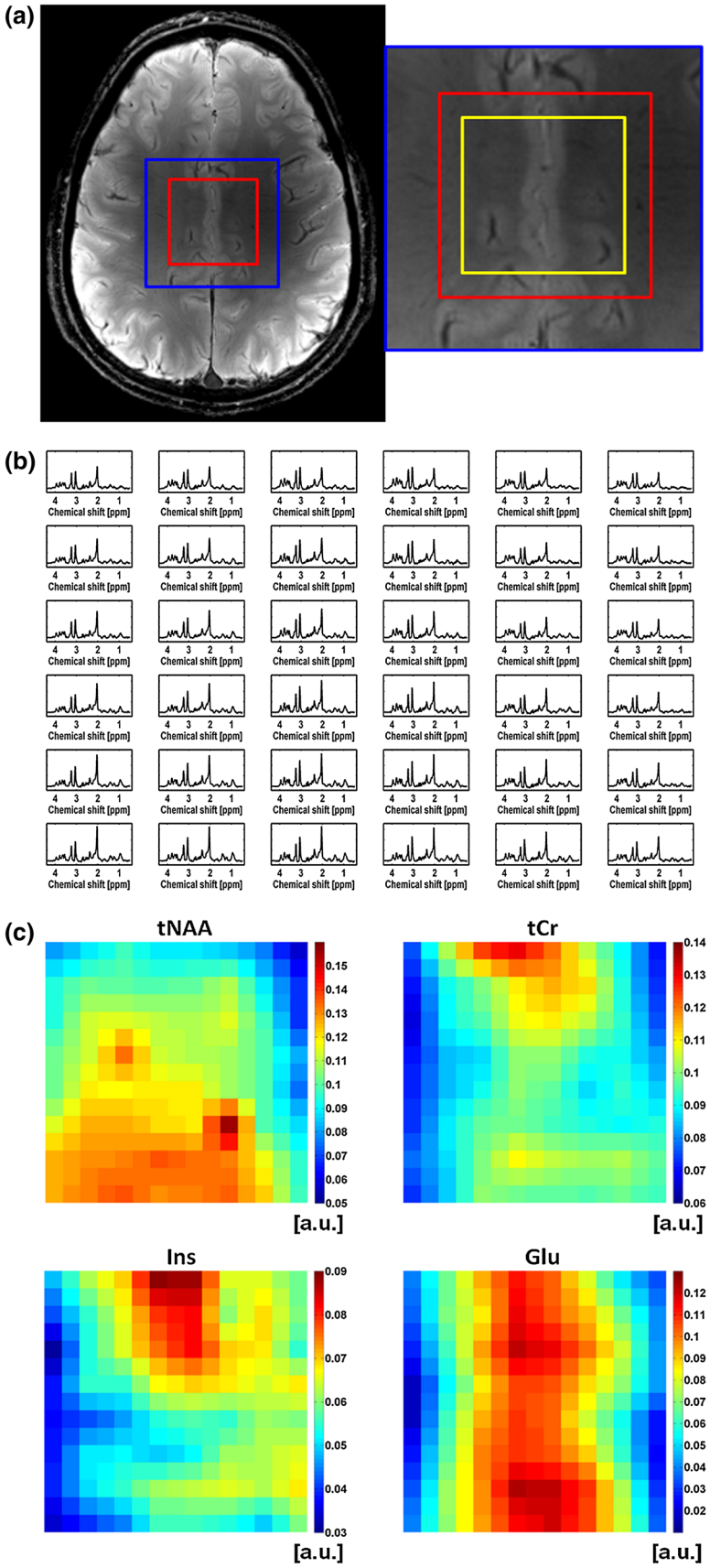

Fig. 3 An example of spectra and metabolite maps acquired for a representative volunteer at higher resolution (32 × 32 voxels, nominal voxel size: 5 × 5 × 15 mm^3) and with a 16-channel transmit/31-channel receive coil. The *blue square* indicates the MRSI-VOI, whereas *yellow* and *red squares* correspond to a 6 × 6 and an 8 × 8 voxel area from which spectra (**b**) and metabolite maps (**c**) are shown below. The presented spectra (**b**) were zero-filled to 4,096 complex data points, apodized with a Hanning function (time constant 400 ms) and phase and baseline corrected. The average SNR and FWHM for the tCr peak across the displayed 6 × 6 voxel area (marked with *yellow square*) were 24.7 ± 1.6 and 15.4 ± 06 Hz, respectively. Metabolite maps at the *bottom* (**c**) were calculated based on the apparent concentration values found with LCModel for a central 8 × 8 voxel area (marked with *red square*). Before the quantification, all the spectra were eddy current corrected (done in LCModel as preprocessing step). No additional offline spectral post-processing was applied

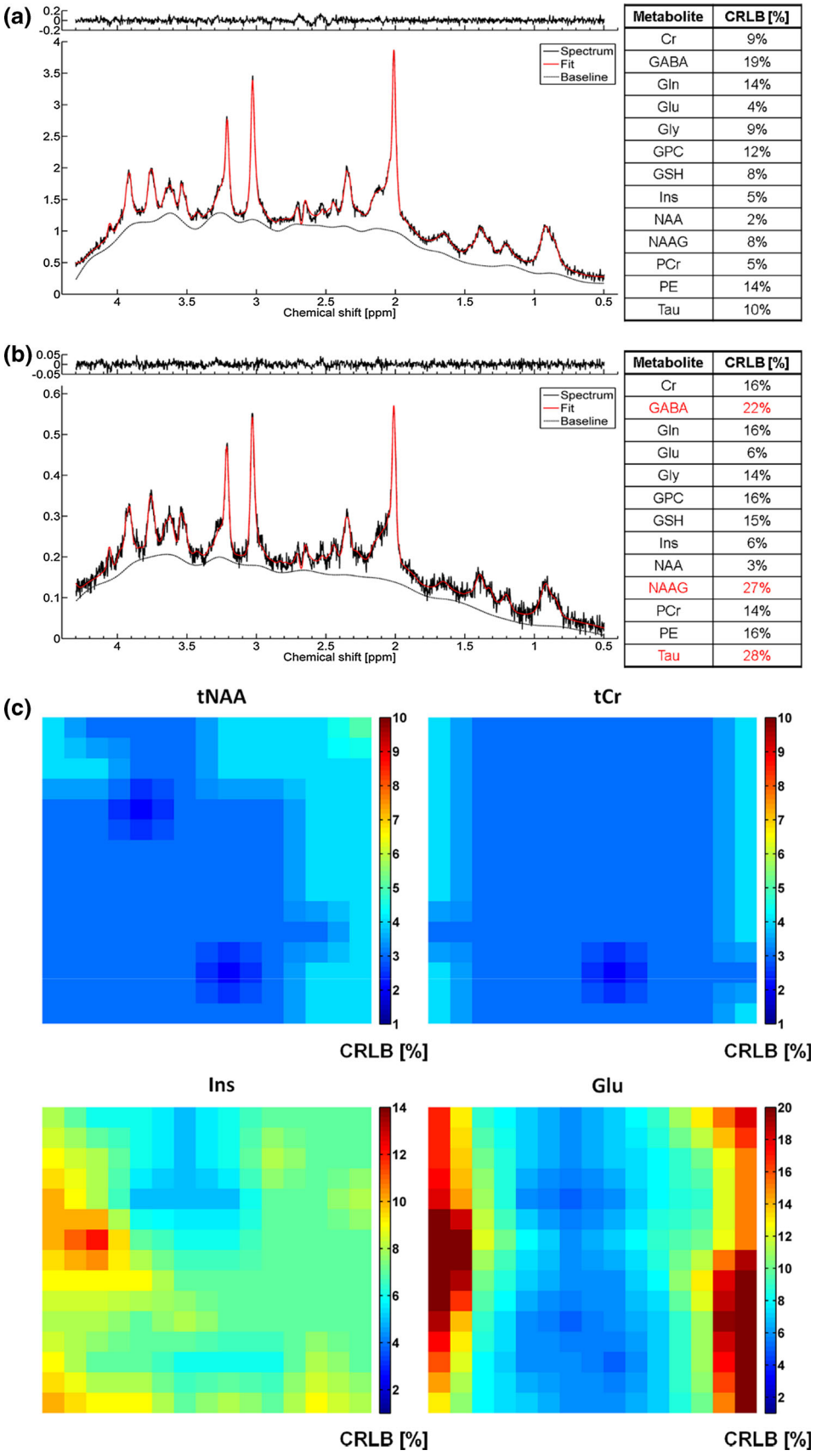

Fig. 4 Examples of MRSI spectra as quantified by LCModel (**a**, **b**) and CRLB maps calculated for tNAA, tCr, Ins and Glu (**c**). In the upper part spectra acquired with an 8-channel transmit/24-channel receive coil (**a**—resolution 16×16 voxels, nominal voxel size: 10 mm^3 isotropic) and a 16-channel transmit/31-channel receive coil (**b**—resolution 32×32 voxels, nominal voxel size: $5 \times 5 \times 15$ mm^3) are compared. The *tables* on the *right* show the CRLBs as returned by LCModel. Before the quantification, all the spectra were eddy current corrected (done in LCModel as preprocessing step). No additional offline spectral post-processing was applied. In this case, SNR and FWHM values calculated for tCr peak in both spectra (**a**, **b**) were 75.1 and 13.9 Hz; and 30.1 and 13.4 Hz, respectively. Below (**c**), CRLB maps for a central 8×8 voxel area acquired at higher spatial resolution are shown

Table 1 Average metabolite concentrations and CRLBs of the central 2 × 2 voxels for all volunteers measured with the 8-channel transmit/24-channel receive coil (20 spectra in total), as returned by LCModel. The standard deviations provide information about intra-volunteer differences

Metabolite	Average concentration (mmol/kg)	SD (mmol/kg)	Average CRLB (%)	SD (%)
Cr	3.2	±0.4	10.1	±1.1
GABA	1.4	±0.3	17.2	±2.7
Gln	1.4	±0.3	18.9	±4.5
Glu	8.5	±1.1	4.5	±0.6
Gly	1.7	±0.3	10.5	±1.4
GSH	1.7	±0.2	9.9	±1.0
Ins	4.6	±0.5	5.0	±0.3
NAA	9.8	±1.3	2.2	±0.4
NAAG	1.4	±0.4	15.8	±10.8
PCr	5.1	±0.8	7.1	±1.1
PE	1.3	±0.2	13.5	±1.7
Tau	1.6	±0.4	13.2	±2.3
GPC + PCho	1.0	±0.2	11.3	±3.4
NAA + NAAG	11.2	±1.6	2.4	±0.5
Ins + Gly	6.3	±0.7	4.3	±0.4
Cr + PCr	8.3	±1.0	2.0	±0.0
Glu + Gln	9.9	±1.3	5.1	±0.6

for tNAA, tCr (CRLB $\leq$ 6 %) and for Ins (CRLB $\leq$ 12 %), which indicates especially robust fit for those metabolites. In the case of Glu, CRLB values for the voxels at the edges of the evaluated part of the VOI were greater than 20 %, but below 12 % in the central regions.

The LCModel quantification results for the measurements with the shortest RF pulse duration (1,400 μs) are summarized in Table 1, where the average values of absolute metabolite concentrations and CRLBs across all the measured volunteers are listed. Table 1 confirms the above observations (Fig. 4), and that for all the measured volunteers, it was possible to quantify at least 12 metabolites with CRLB below 20 %.

Discussion

In this study, we have demonstrated that in vivo MRSI of the human brain at a field strength of 9.4 T is feasible. While all measured spectra are of decent quality, direct comparison with other studies is rather difficult, mainly because of differences in hardware and sequence parameters, but also due to the limited number of scientific reports describing in vivo MRS of the human brain at this field strength [11]. Regardless of the above, spectra presented here show good agreement in terms of spectral quality with data published previously [11]. As for metabolite quantification, we were able to assess 12 metabolites, whereas Deelchand et al. [11] reported quantification of 15 metabolite resonances. Slight differences in metabolite concentrations and CRLB observed between our own and previous results [11] could be caused by differences in the echo time used (20 vs. 8 ms), voxel size, voxel localization (superior part of the brain vs. occipital lobe) and the remaining CSDE in slice direction.

Reasonable spectral quality and SNR allowed for reliable quantification of 12 metabolite resonances (CRLB $<$ 20 %), including small or heavily overlapping ones (i.e., Gly, GSH, PE, Tau, Cr, PCr, NAA and NAAG) for all volunteers. However, the fitting residuals show the presence of remaining signals between $\sim$2.4 and $\sim$2.8 ppm, which correspond to the resonances of Gln and NAA (at $\sim$2.6 ppm). Since the CRLBs for Gln were relatively high, this may indicate underestimation of those particular resonances (Fig. 4), and could be a consequence of the remaining influence of CSDE in the slice-selection direction or due to the overlap with broad macromolecules signals, as those were simulated with LCModel standard parameters. Thus, the fitting performance could be improved by refinement of the basis set, and in the latter case, by including the in vivo measured baseline in the quantification routine [24] and by modification of some of the LCModel's control parameters, particularly DKNTMN (controls the knot spacing for the baseline spline fitting) and DESDSH (responsible for uncertainty in referencing between the measured spectrum and the basis-set), as described in [5]. However, further in vivo and phantom experiments would be required for determining the impact of both aforementioned factors on the precision of metabolite quantification. Furthermore, relatively high value of the average CRLB for GABA calculated across all the measured subjects (Table 1—17.2 ± 2.7 %) suggests that although the previous studies conducted at 7 T demonstrated reliable detection of GABA with the use of short TE STEAM [2, 5, 12] and SPECIAL [6] techniques, the use of spectral editing methods [25, 26] at 9.4 T may certainly be a valuable alternative. Regardless of the above, the absolute metabolite concentrations were in reasonable agreement with the results published previously for 9.4 T [11]. The largest differences in metabolite concentrations between the current and previous study [11] were obtained for Gln ($\sim$35 %) and GSH ($\sim$50 %). For most of the metabolites, however, the differences in the concentrations were not larger than 30 % (NAA, NAAG, PE, Tau) or even smaller than 15 % (Cr, GABA, Glu, Ins, PCr). On the other hand, in most cases, the differences in CRLB were below 5 %, with the exception of the CRLB value obtained for Gln (12 %). This suggests that the observed differences in metabolite concentrations could be mainly attributed to

differences in the echo time and VOI localization used in the current and a previous study [11]. Also, the concentrations of tNAA, tCho, tCr, Ins, and Glx were similar to those reported at 1.5 [27, 28] and 3 T [6]. Moreover, despite of being influenced by B_1 field inhomogeneities and remaining CSDE, the metabolite maps presented in Fig. 3 show the spatial distribution of metabolite concentrations to be similar to those reported at 7 T [4, 14]. Slight differences in values and spatial distribution of metabolite concentrations could be explained by tissue heterogeneity of spectroscopy voxels (mixture of white and gray matter), relatively large age dispersion of the examined group of volunteers (age ranged from 27 to 44 years old), differences in coil sensitivity, echo time used during MRSI acquisition, and finally, by residual influences of T_1 weighting on the metabolite concentrations.

In this study, the average linewidth calculated for tCr across all the measured subjects was 14.7 ± 1.4 Hz, while Deelchand et al. [11] reported ~13 Hz. This difference could be explained by the use of the vendor provided, field-map based shimming algorithm, which may not lead to optimal results in the examined region, and by the larger shim volume required for MRSI ($60 \times 60 \times 10$ and $60 \times 60 \times 15$ mm^3) in contrast to single voxel spectroscopy ($20 \times 20 \times 20$ mm^3). Improving the B_0 homogeneity by improved shimming would be an important factor for increasing spectral quality, especially since the inhomogeneities of the B_0 field are known to become more serious at higher fields. The 9.4 T scanner used in this study was equipped with up to second order shims with sufficient strengths (linear: 5 mT/m, Z^2: 9.4 mT/m^2, ZX: 4.7 mT/m^2, ZY, X^2–Y^2, XY: 4.5 mT/m^2) for this application. The shim algorithm did not reach the limits in any of the shim channels for any subject, since the selected brain region imposed rather 'benign' shimming conditions. Quantification could thus be further enhanced by higher order B_0 shimming, which would decrease the spectral linewidth and reduce the overlap between adjacent metabolite resonances. Recent studies show that up to fourth-order shimming significantly increases the homogeneity of the B_0 field, and hence improves the spectral resolution [29]. Since only second order shims were available in this study, MRSI spectra from the central part of the brain were acquired, where B_0 is expected to be relatively homogeneous. Additional improvements in homogeneity of the B_0 field could be also achieved with the use of automated B_0 shimming algorithms such as ROI based shim methods [30], methods based on the use of field maps acquired with gradient-echo sequence (GRESHIM) [31], or on sampling of the magnetic field with a limited number of projections (FASTMAP) [32, 33], as the performance of those have been shown to be superior when compared with the vendor provided shimming algorithms [34, 35].

Due to its strong dependence on field strength, CSDE is one of the major issues in ultra-high field MR spectroscopy in humans, since the limited RF power and the B_1 inhomogeneities pose strong restrictions on the duration and thus the bandwidth of the excitation pulses. Using MRSI instead of single voxel spectroscopy can in part solve this problem, since only the voxels at the edges of the VOI are affected. When these outer voxels are discarded, the remaining data will not be impaired by in-plane CSDE. The remaining effect in slice direction was minimized by using the shortest possible pulse duration, which was only able to reduce CSDE in this dimension to 39 and 57 % for the measurements at RF duration of 1,400 (8-channel Tx coil) and 1,800 μs (16-channel Tx coil), respectively. Using a three-dimensional MRSI technique could also remove the displacement in the slice direction; however, this may come with an excessive increase in scan duration. Using conventional adiabatic pulses for excitation is limited because of the long duration and high power for these pulses in the strongly inhomogeneous transmit field at ultra-high field, which might cause timing and SAR problems [13, 36]. The latter could be minimized with the use of gradient offset independent adiabatic pulses (GOIA), as proposed by Andronesi et al. [37]. However, since the GOIA pulses are of relatively long duration (3.5 ms per pulse), full localization might still prolong minimal achievable echo time [37]. On the other hand, localization by outer volume suppression (FIDLOVS) may be an alternative if limitations from the highly inhomogeneous B_1 field at 9.4 T can be overcome [4, 14].

Another issue at ultra-high field is the homogeneity of the B_1 field. Recent studies have demonstrated that homogeneity of the transmit field may be improved by RF shimming [36, 38–40], by using RF pulses that are less sensitive to the spatial distribution of the transmit field [4, 13, 14], or by a combination of both [41]. However, since the use of multi-transmit capabilities in in vivo human studies has not been clarified by the local ethics board, RF shimming was not available for these measurements. Therefore, for minimizing the influence of B_1^+ inhomogeneities, the VOI for MRSI was placed in the central part of the brain, so that it covered an area with a relatively high amplitude of the transmit field (Fig. 1). Subsequently, the flip angle value measured with the AFI sequence and used for the correction of the reference voltage was taken as a mean over the region that was slightly bigger than the VOI of the MRSI. This allowed calibration of the voltage necessary for water suppression and VOI-selection RF pulses. However, the optimization of the OVS pulses was significantly restricted, as those cover a more extensive area of the brain, with B_1 inhomogeneities being larger. Moreover, a significant difference in the amplitude and SNR of resonances from the VOI's center and edges was observed.

This also reduced the amount of information about the spatial distribution of metabolite concentrations and suggests that an additional effort toward homogenization of B_1^+ should be made.

Regardless of the use of STEAM, where only a half of the available signal is acquired, all MRSI spectra show reasonable spectral quality. The average SNR calculated across all the measured volunteers was, however, slightly lower than the SNR reported in previous studies performed at 7 T [2, 5, 40] and 9.4 T [11] with the use of the STEAM sequence. This may be explained by the differences in total scan time, voxel size and position, sensitivity of the receive coil, relatively long TE used in our measurements, and finally, by the influence of inhomogeneities in both B_1^+ and B_0 magnetic fields. Further increase in SNR could be achieved either by shortening the TE, which could be realized with asymmetric sinc RF pulses as described in [11], or by using alternative acquisition schemes, for instance based on spin-echo excitation [6, 39, 42], localization with adiabatic refocusing pulses [3, 42], or with OVS only [4, 14]. Those approaches, however, require relatively high RF peak power and thus increase total SAR, which has to be compensated by using longer TR. In addition, this often leads to prolonged TE, as the used RF pulses are long (especially adiabatic pulses). In contrast, the STEAM sequence needs less RF power and can be optimized to provide much shorter TE [5, 11, 12, 36, 43], thus enabling detection of fast relaxing metabolites.

Conclusion

For this initial experience with MRSI summarized in this report, only conventional techniques as applied for 3 T and below were used. The limitations found in these measurements, especially concerning CSDE, B_0 and B_1 inhomogeneities, however, demonstrate the necessity of applying further modern and innovative approaches, as presented in recent publications for field strengths of 7 T and above [4, 11, 14]. Thus, further studies are needed in order to assess the possible increase in SNR and spectral resolution at 9.4 T compared to 7 T. Nevertheless, spectra acquired for all volunteers were of good quality and allowed quantification of 12 metabolites, some of which are heavily overlapped at field strengths below 7 T (like Glu, Gln, NAAG or Tau), or have small concentrations (particularly: PE, GSH, GPC and Gly).

Acknowledgments This work was founded (in part) by the Helmholtz Alliance ICEMED—Imaging and Curing Environmental Metabolic Diseases, through the Initiative and Networking Found of the Helmholtz Association.

Conflict of interest The authors declare that they have no conflict of interest.

Ethical standard All volunteer studies have been approved by the local ethics committee and have therefore been performed in accordance with the ethical standards laid down in the 1964 Declaration of Helsinki and its later amendments.

Informed consent All in vivo measurements described in this study were conducted exclusively on healthy volunteers. All volunteers gave their informed consent prior to their inclusion in the study.

References

1. Pohmann R, Shajan G, Balla DZ (2011) Contrast at ultra-high field: relaxation times, magnetization transfer and phase in the rat brain at 16.4 T. Magn Reson Med 66:1572–1581
2. Tkac I, Gruetter R (2005) Methodology of ^{1}H NMR spectroscopy of the human brain at very high magnetic fields. Appl Magn Reson 29(1):139–157
3. Marjanska M, Auerbach EJ, Valabregue R, de Moortele Van, Adriany G, Garwood M (2012) Localized ^{1}H NMR spectroscopy in different regions of human brain in vivo at 7 T: T_2 relaxation times and concentrations of cerebral metabolites. NMR Biomed 25:332–339
4. Henning A, Fuchs A, Murdoch JB, Boesinger P (2009) Slice-selective FID acquisition, localized by outer volume suppression (FIDLOVS) for ^{1}H-MRSI of the human brain at 7 T with minimal signal loss. NMR Biomed 22:683–696
5. Tkac I, Oez G, Adriany G, Ugurbil K, Gruetter R (2009) In-vivo ^{1}H NMR spectroscopy of the human brain at high magnetic fields: metabolite quantification at 4T vs. 7T. Magn Reson Med 62:868–879
6. Mekle R, Mlynarik V, Gambarota G, Hergt M, Krueger G, Gruetter R (2009) MR spectroscopy of the human brain with enhanced signal intensity using ultrashort echo times on a clinical platform at 3T and 7T. Magn Reson Med 61:1279–1285
7. Yang S, Hu J, Kou Z, Yang Y (2008) Spectral simplification for resolved glutamate and glutamine measurement using a standard STEAM sequence with optimized timing parameters at 3, 4, 4.7, 7 and 9.4 T. Magn Reson Med 59:236–244
8. Choi C, Dimitrov I, Douglas D, Zhao C, Hawesa H, Ghose S, Tamminga CA (2009) In vivo detection of serine in the human brain by proton magnetic resonance spectroscopy (^{1}H MRS) at 7 T. Magn Reson Med 62:1042–1046
9. Banerjee A, Ganji S, Hulsey K, Dimitrov I, Maher E, Ghose S, Tamminga C, Choi C (2012) Measurement of glycine in gray and white matter in the human brain in vivo by ^{1}H MRS at 7 T. Magn Reson Med 68:325–331
10. Pan JW, Avdievich N, Hetherington HP (2010) J-refocused coherence transfer spectroscopic imaging at 7 T in human brain. Magn Reson Med 64:1237–1246
11. Deelchand DK, Van de Moortele PF, Adriany G, Iltis I, Andersen P, Strupp JP, Vaughan T, Ugurbil K, Henry PG (2010) In-vivo ^{1}H NMR spectroscopy of the human brain at 9.4 T: initial results. J Magn Reson 206:74–80
12. Tkac I, Andersen P, Adriany G, Merkle H, Ugurbil K, Gruetter R (2001) In vivo ^{1}H NMR spectroscopy of the human brain at 7T. Magn Reson Med 46:451–456
13. Boer VO, Siero JCW, Hoogduin H, van Gorp JS, Luijten PR, Klomp DWJ (2011) High-field MRS of the human brain at short TE and TR. NMR Biomed 24:1081–1088

14. Bogner W, Gruber S, Trattnig S, Chmielnik M (2012) High-resolution mapping of human brain metabolites by free induction decay ^{1}H MRSI at 7T. NMR Biomed 25:873–882
15. Shajan G, Kozlov M, Hoffman J, Turner R, Scheffler K, Pohmann R (2013) A 16-channel dual-row transmit array in combination with a 31-element receive array for human brain imaging at 9.4 T. Magn Reson Med 71:870–879
16. Ogg RJ, Kingsley RB, Taylor JS (1994) WET, a T_1 and B_1 insensitive water suppression method for in vivo localized ^{1}H NMR spectroscopy. J Magn Reson B 104(1):1–10
17. Yarnykh VL (2007) Actual flip-angle imaging in the pulsed steady state: a method for rapid three-dimensional mapping of the transmitted radiofrequency field. Magn Reson Med 57:192–200
18. Pohmann R, Scheffler K (2013) A theoretical and experimental comparison of different techniques for B_1 mapping at very high fields. NMR Biomed 26:265–275
19. De Graaf RA (2007) Radiofrequency Pulses. In: De Graaf RA (ed) In vivo NMR spectroscopy, 2nd edn. Wiley, Chichester, pp 233–293
20. Provencher SW (1993) Estimation of metabolite concentrations from localized in vivo proton NMR spectra. Magn Reson Med 30:672–679
21. Govindaraju V, Young K, Maudsley AA (2000) Proton NMR chemical shifts and coupling constants for brain metabolites. NMR Biomed 13:129–153
22. Tkac I (2008) Refinement of simulated basis set for LCModel analysis. In: Proceedings of the 16th scientific meeting, International Society for Magnetic Resonance in Medicine, Toronto, p 1624
23. Ernst T, Kreis R, Ross BD (1993) Absolute quantitation of water and metabolites in the human brain. I. Compartments and water. J Magn Reson Ser B 102:1–8
24. Hong ST, Balla DZ, Shajan G, Choi C, Ugurbil K, Pohmann R (2011) Enhanced neurochemical profile of the rat brain using in vivo ^{1}H NMR spectroscopy at 16.4 T. Magn Reson Med 65:28–34
25. Terpstra M, Ugurbil K, Gruetter R (2002) Direct in vivo measurement of human cerebral GABA concentration using MEGA-editing at 7T. Magn Reson Med 47:1009–1012
26. Andreychenko A, Boer VO, de Castro CSA, Luijten PR, Klomp DWJ (2012) Efficient spectral editing at 7T: GABA detection with MEGA-sLASER. Magn Reson Med 68:1018–1025
27. Helms G (2000) A precise and user-independent quantification technique for regional comparison of single volume proton MR spectroscopy of the human brain. NMR Biomed 13:398–406
28. Wang Y, Li SJ (1998) Differentiation of metabolic concentrations between gray matter and white matter of human brain by in vivo 1H magnetic resonance spectroscopy. Magn Reson Med 39:28–33
29. Pan JW, Lo KM, Hetherington HP (2012) Role of high order and degree B_0 shimming for spectroscopic imaging of the human brain at 7 Tesla. Magn Reson Med 68:1007–1017
30. Hetherington HP, Chu WJ, Gonen O, Pan JW (2006) Robust fully automated shimming of the human brain for high-field ^{1}H spectroscopic imaging. Magn Reson Med 56:26–33
31. Shah S, Kellerman P, Greiser A, Weale PJ, Zuehlsdorff S, Jerecic R (2009) Rapid fieldmap estimation for cardiac shimming. In: Proceedings of the 17th scientific meeting, International Society for Magnetic Resonance in Medicine, Honolulu, Hawaii, USA, p 566
32. Gruetter R (1993) Automatic, localized in vivo adjustment of all first- and second-order shim coils. Magn Reson Med 29:804–811
33. Gruetter R, Tkac I (2000) Field mapping without reference scan using asymmetric echo-planar techniques. Magn Reson Med 43:319–323
34. Zhong X, Lyubich YM, De Vito T, Shah S, Knight-Scott J (2012) Improving in vivo 1H-MRS with robust automated shim techniques: a comparison study of FASTESTMAP and GRESHIM. In: Proceedings of the 20th scientific meeting, International Society for Magnetic Resonance in Medicine, Melbourne, Victoria, Australia, p 4397
35. Zhong X, Lyubich YM, De Vito T, Shah S, Knight-Scott J (2013) Quantitative comparison of shim algorithms for in vivo ^{1}H-MRS. In: Proceedings of the 21th scientific meeting, International Society for Magnetic Resonance in Medicine, Salt Lake City, Utah, USA, p 3988
36. Avdievich NI, Pan JW, Beahring JM, Spencer DD, Hetherington HP (2009) Short echo spectroscopic imaging of the human brain at 7 T using transceiver arrays. Magn Reson Med 62:17–25
37. Andronesi OC, Gagoski BA, Sorensen AG (2012) Neurologic 3D MR spectroscopic imaging with low-power adiabatic pulses and fast spiral acquisition. Radiology 262(2):647–661
38. Hetherington HP, Avdievich NI, Kuznetsov AM, Pan JW (2010) RF shimming for spectroscopic localization in the human brain at 7 T. Magn Reson Med 63:9–19
39. Boer VO, van Lier ALHMW, Hoogduin JM, Wijnen JP, Luijten PR, Klomp DWJ (2011) 7-T ^{1}H MRS with adiabatic refocusing at short TE using radiofrequency focusing with a dual-channel volume transmit coil. NMR Biomed 24:1038–1046
40. Emir UE, Auerbach EJ, Van de Moortele PF, Marjanska M, Ugurbil K, Terpstra M, Tkac I, Oez G (2012) Regional neurochemical profiles in the human brain measured by ^{1}H MRS at 7 T using local B_1 shimming. NMR Biomed 25:152–160
41. Boer VO, Klomp DWJ, Juchem C, Luijten PR, de Graaf RA (2012) Multislice ^{1}H MRSI of the human brain at 7 T using dynamic B_0 and B_1 shimming. Magn Reson Med 68:662–670
42. Zhu H, Soher B, Ouwerkerk R, Schaer M, Barker PB (2013) Spin-echo magnetic resonance spectroscopic imaging at 7T with frequency-modulated refocusing pulses. Magn Reson Med 69:1217–1225
43. Tkac I, Starcuk Z, Choi IY, Gruetter R (1999) In vivo ^{1}H NMR spectroscopy of rat brain at 1 ms echo time. Magn Reson Med 41:649–656